Mechanism of anomalously increased oil displacement with aqueous viscoelastic polymer solutions

Andrew Clarke, Andrew M Howe, Jonathan Mitchell, John Staniland, Laurence Hawkes, Katherine Leeper
Schlumberger Gould Research, Cambridge, UK

Supporting Material

1 Core flood experimental detail

The cores used to obtain the data in Figures 1a and 1b of the paper were Bentheimer, an outcrop sandstone. Samples were cut, 37.9mm in diameter and 50.7mm in length, washed in deionised water and dried in an oven overnight at 60°C.

Bentheimer has a uniform texture with large grains. The pore throat distribution from mercury intrusion porosimetry[i] is well characterised by a single peak showing a median diameter ~38.8 μm.[ii] The porosity 0.232, pore volume (PV) 13.2 cm^3 and gas permeability (k_g) 2680 mD (≈ 2.6 μm^2) of the core-plug were determined using a helium expansion porosimeter, steady-state gas (nitrogen) permeameter and a high pressure core holder [ErgoTech, Conwy, UK]. The brine permeability (k_w) was 1.8 D, giving a ratio of k_g/k_w of ~ 1.5, which is in good agreement literature data on sandstones of a wide range of permeability[iii]. The apparent viscosity values plotted in Fig 1b were calculated using k_g.

A synthetic brine representative of a particular practical flooding fluid was used in all the experiments presented. The formulation is listed in Table 1. The prepared brine was passed through a 0.22μm filter and degassed. Rheological and single phase flow experiments when also performed with simple NaCl solutions or other simple brines with the same ionic strength and showed the same results. Here we present a consistent set of compositions for consistency.

Salt	Concentration / mg L^{-1}	Concentration / mmol L^{-1}		Ion	Concentration / mg L^{-1}	Concentration / mmol L^{-1}
NaCl	3115	53.30		Na^+	1660	72.21
$NaHCO_3$	1310	15.60		K^+	28.3	0.72
Na_2SO_4	239	1.67		Ca^{2+}	26.2	0.65
KCl	54	0.72		Mg^{2+}	5.5	0.46
$CaCl_2.2H_2O$	96	0.65		SO_4^{2-}	160	1.67
$MgCl_2.6H_2O$	93	0.46		Cl^-	1994	56.24
				HCO_3^-	951	15.60

Table 1: Composition of synthetic brine; Total dissolved solids approximately 4800 ppm. Concentrations of salts and resultant ionic concentrations are given. Salts were added to solution in the order presented (top to bottom).

The cores were initially evacuated to 200Pa and then saturated with the synthetic brine.

For single phase core floods the cores were then mounted horizontally in a conventional core holder (Temco) and confined at 80 bar. Fluids were pumped using an ISCO 260D displacement pump (Teledyne) over a range of flow rates. The pressure drop along the core was monitored using a range of pressure transducers, both differential and gauge, to adequately cover the dynamic range required (33-X series, Keller).

For multiphase floods, the saturated cores were mounted in a custom core holder designed for use with a 2.4 MHz NMR system (Oxford Instruments; model "Big-2", with a Maran DRX-TCP console). Details of this instrument are given elsewhere.[iv] Again fluids were pumped using ISCO 260D or 1000D pumps and pressures monitored using a range of gauges (33-X series Keller).

Outcrop Bentheimer sandstone is expected to be water wet. The wettability state was estimated using the Amott method,[v] where an oil saturated plug was seen to rapidly imbibe water. Further confirmation of the wettability state was obtained from NMR relaxation measurements.[vi,vii] Brine was observed to undergo enhanced relaxation on contact with the pore surface, whereas the oil did not (in the presence of residual brine), indicating the rock surface was strongly water wet.

For multiphase core desaturation experiments the initially brine saturated core was flooded with 20PV of oil (S20, PSL Rheotek) at 10ml/min which achieved a saturation S_O=96%. Then a brine flood was initiated at 0.2ml/min for approximately 20PV which brought the oil saturation to a residual value of S_{OR}≈64%. [Note that further flooding of brine for 75PV did not further reduce S_{OR}. Throughout this study, the values of initial oil saturation, the oil permeability at this saturation and the residual oil saturation after the 0.2 ml/min flood remained essentially unchanged.] At this point a macroscopically reproducible initial state was achieved. Further floods with either brine or polymer solution at successively increasing injection flow rates were then performed whilst continually monitoring pressure.

The interfacial tension IFT of the oil against the synthetic brine was measured at various stages of the experiment and found to be 0.94mN/m ± 0.08mN/m. The polymers used are not seen to change the liquid-liquid interfacial tension of the system.

2 Polymer solution preparation

Two types of polymer were used: hydrolysed poly(acrylamide) (HPAM), a synthetic polymer, and xanthan a polysaccharide. The HPAM adopts a very flexible random-coil conformation in solution. In contrast, xanthan is mostly in a double-helix form, which gives significant rigidity to the molecule.

The HPAM samples were supplied by SNF Floerger as Flopaam 3630S (batch UE4353) and Flopaam 3130S (batch 99092-C) and are reported by the supplier to have mean molecular weight (MW) values 18 - 20 MDa and 3.6 MDa, respectively. Both HPAMs have 30 mole% of the acrylamide groups hydrolysed to the acid form. The xanthan sample was supplied by International Drilling Fluids IDF and its mean molecular weight is not known. The polymers are dispersed in the synthetic brine.

A 2 L stock solution of each of the polymers was made up, by dissolving in the synthetic brine. To prevent biological or oxidative degradation of the polymer ITW preservative package (15 wt% isopropanol, 7.5 wt% thiourea and 77.5wt% water), was added to each stock solution at mass two-thirds that of the dry mass of the polymer.

For each stock solution, the Brine and ITW package were weighed out and an overhead stirrer used to stir the solution. The dry polymer was added carefully to the solution over fifteen seconds. (If the polymer is added too rapidly insoluble lumps can form) while if the polymer is added too slowly the solution would become too viscous and the last of the dry polymer added would not dissolve). After mixing the polymer solutions on the overhead stirrer for an hour to ensure the polymer was fully dispersed, the bottles of solution were rolled for 48 hours to promote gentle mixing.

The HPAM solutions were optically clear and they were passed (pulled under low pressure) through a filter cloth with pore size 35 µm to remove any polymer agglomerates and particulates from the solution. The stock solutions were stored in a fridge to help prevent degradation of the polymer prior to use.

The stock xanthan solution was cloudy, so it was placed on the bottle roller for a further 72 hours at 65^{o}C to aid dissolution. After filtration, the xanthan solution was placed in an oven at 60^{o}C for a further 24 hours and it underwent a series of sequential filtrations under pressure through 22 µm, 16 µm and 8 µm filters (all Whatman 540) to remove any remaining polymer aggregates or undissolved microgel. Once the xanthan had cooled to room temperature, the stock solution was also stored in the fridge.

The final HPAM solutions appeared to be completely transparent, while the xanthan solutions were slightly cloudy.

3 Microfluidic networks

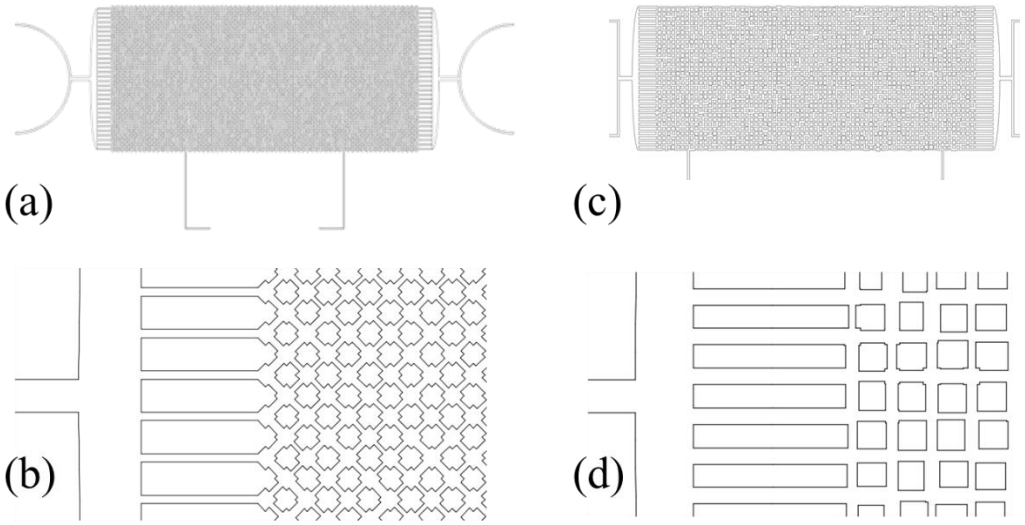

Figure 1 Microfluidic network geometries. In all cases the channel depth is 100µm (a) MM2 complete microfluidic network. Two pressure taps are provided along the edge of the device. (b) MM2 close-up of section near the inlet of the device. (c) MM1 complete microfluidic network. (d) MM1 close-up near inlet of the device.

Our microfluidic networks are simple 2D representations of porous structures, Figure 1. Data from two devices are included in the paper: MM1 consisting of nodes (pores) or a square grid connected by channels (pore throats) with a randomised width about 80µm. The channels were aligned with the flow direction and the normal to the flow direction. Early in our work it was realised that having channels aligned with the flow tended to suppress the effects that are investigated in this work. Thus a second network was designed, MM2, with the basic pattern rotated 45° with respect to the average flow direction. This network has nodes (pores) which are square of side 200µm, and channels (pore throats) of width randomly

distributed about 75μm with a lower cutoff of 50μm and an upper cutoff of 150μm. All devices are manufactured by Epigem Ltd. As supplied, the channels have SU8 internal surfaces and thus are hydrophobic.

4 Particle Tracking Velocimetry

The velocity fluctuation data shown in figure 3 was derived from conventional particle tracking velocimetry measurements obtained using a high-speed camera (Photron MX2). The flow is seeded with 1μm polystyrene particles (Sigma-Aldrich) and images are captured using a high-speed video camera. The lens systems has a moderately high numerical aperture (Navitar) giving a depth of focus approximately the middle third of the microfluidic channel. Analysis of the image sequences (LabView) provide spatial liquid velocity measurements. No attempt was made to resolve the velocity normal to the network plane.

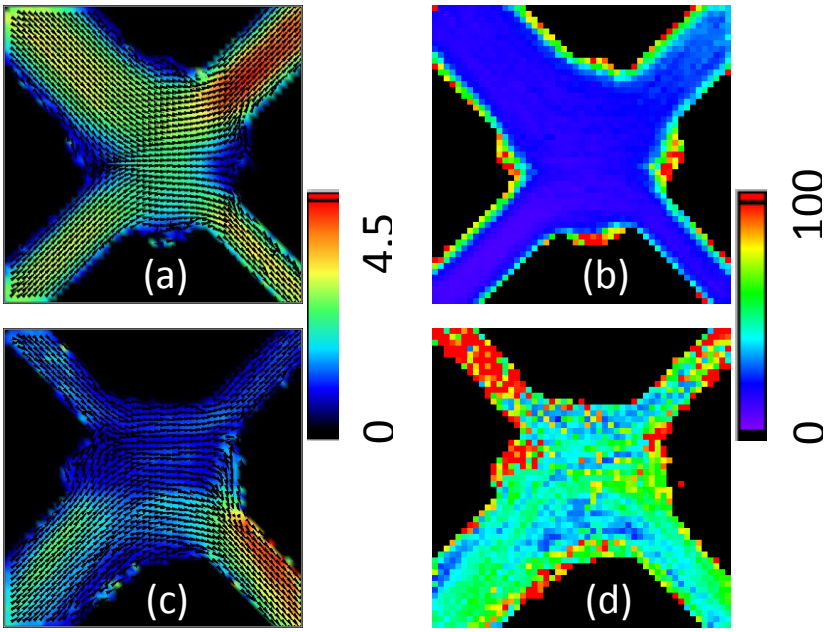

Figure 2 Particle tracking velocimetry images. (a) and (c) show velocity maps for 84wt% aqueous glycerol and 0.12wt% aqueous polyacrylamide (3630S). The mean flow rate in the micromodel was 27μl/min. (b) and (d) show the corresponding standard deviation of the measured time varying local speed. The high standard deviation along the channel walls reflects low particle statistics. The very large fluctuations within the channel in (d) reflect the strongly time-varying local speed.

The liquid velocity measurements in each frame of the image sequence are randomly distributed across the image. These are then either (i) binned onto a regular square grid allowing average speeds and standard deviations over the whole image sequence to be obtained as in Figure 2, or (ii) an area is selected and the time varying average speed within that area plotted Figure 3. For case ii (which is the method used for calculating the data in Figure 3 of the main-body text), the area must be sufficiently large so as to minimise the contribution to statistical noise that arise from the (small) number of particles within any frame.

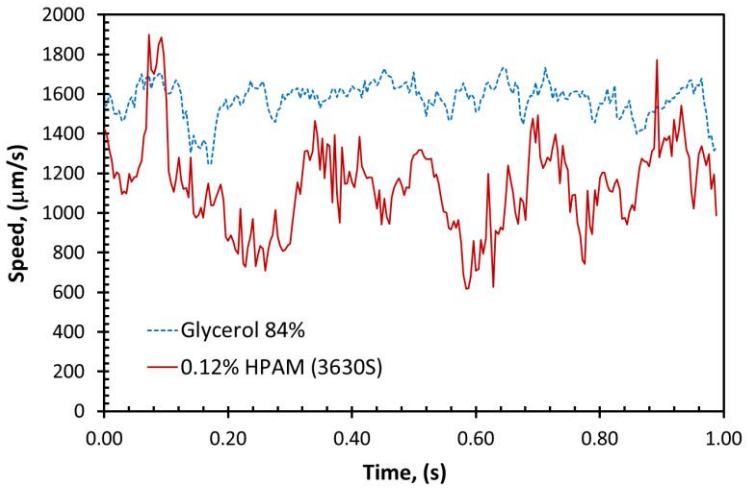

Figure 3 Fluctuation in the average speed within a central 100μm x 100μm square in the centre of the network node (pore) shown in Figure 2. The concentration of particles used in the two experiments was the same. The fluctuation observed in the glycerol case arises from statistic noise whereas that observed in the HPAM case is significantly greater.

5 Video Sequences

The images in figure 4 of the paper are derived from video sequences (4 fps) obtained during the flow of each polymer. The original sequences are attached as 0.24%_xanthan.avi and 0.24%_3630_polyacrylamide.avi. The time varying menisci positions are obvious in the polyacrylamide sequence whereas the menisci are completely stationary in the xanthan sequence despite the same aqueous phase flow rate.

6 Solution rheology

The viscosity-rate dependence of the solutions of HPAM 3630S and xanthan at ≈ 0.12% are given in the body text, the behaviour curves at approximately double concentration of these polymers in solution is shown in figure 5. The measurements (as throughout this work) were at 20°C and made with a bob-and-cup geometry with relatively narrow gap. Again the two polymer solutions have very similar low-shear viscosity and exhibit similar onset and initial power-law shear thinning behaviour. The viscosity at low η(0) has increased by an order of magnitude to ≈ 1 Pa.s (corresponding to $\eta(0) \sim c^{3.3}$) and the behaviour of the two polymer solutions at low shear and at the start of the thinning regime is very similar.

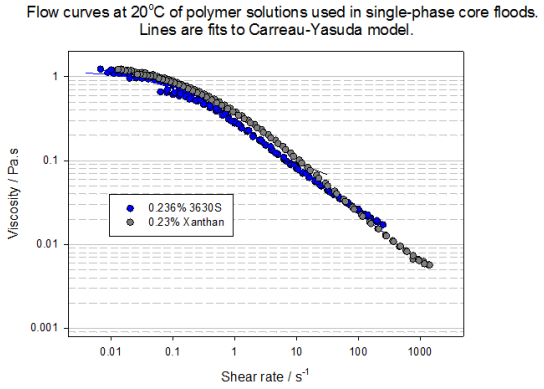

Figure 4 Measured shear rheology of the fluids used for the data shown in figure 4 of the main text.

[i] H. Ritter and L. Drake, 'Pore-size distribution in porous materials' Industrial Eng. Chem., Vol. 17, 1945.

[ii] Measurements and analysis by MCA Laboratories in Meldreth, UK.

[iii] SPE 1-114 I Chatzis, N R Morrow, Correlation of Capillary Number Relationships for Sandstone, SPE Journal 24, 5 *1984.*

[iv] J. Mitchell, J. Staniland, R. Chassagne, and E. J. Fordham, Quantitative in situ enhanced oil recovery monitoring using nuclear magnetic resonance, Transp. Porous Med. **94** (2012) 683-706.

[v] E. Amott, Observations relating to the wettability of porous rock, Trans. AIME **216** (1959) 156-162.

[vi] R. J. S. Brown and I. Fatt, Measurement of fractional wettability of oilfield rocks by the nuclear magnetic relaxation method, Petrol. Trans. AIME **207** (1956) 262-264.

[vii] W. J. Looyestijn and J. P. Hofman, Wettability determination by NMR, SPE Reserv. Eval. Eng. **3** (2006) 146-153.